JACS
JOURNAL OF THE AMERICAN CHEMICAL SOCIETY

ARTICLE

pubs.acs.org/JACS

In-Phase Alignments of Asymmetric Building Units in Ln_4GaSbS_9 (Ln = Pr, Nd, Sm, Gd−Ho) and Their Strong Nonlinear Optical Responses in Middle IR

Mei-Chun Chen,[†,‡] Long-Hua Li,[†] Yu-Biao Chen,[†] and Ling Chen*[,†]

[†]Key Laboratory of Optoelectronic Materials Chemistry and Physics, Fujian Institute of Research on the Structure of Matter, Chinese Academy of Sciences, Fuzhou, Fujian 350002, People's Republic of China

[‡]Graduate School of the Chinese Academy of Sciences, Beijing 100039, People's Republic of China

Supporting Information

ABSTRACT: New noncentrosymmetric rare-earth metal gallium thioantimonates, Ln_4GaSbS_9 were synthesized from stoichiometric element mixtures at 950 °C by high-temperature solid-state reactions. These compounds crystallize in orthorhombic space group *Aba*2 (no.41) with a = 13.799(3)−13.427(5) Å, b = 14.187(3)−13.756(5) Å, c = 14.323(3)−13.954(5) Å, V = 2804(2)−2577 (2) Å^3, and Z = 8 on going from Ln = Pr to Ho. The asymmetric building units, bimetallic polar (Sb_2S_5) units, and dimeric $(GaS_4)_2$ tetrahedra are in-phase aligned as an infinite single anionic chain of $\{[(Ga_2S_6)(Sb_2S_5)]^{10-}\}_\infty$ that is further packed in a noncentrosymmetric pseudolayer motif perpendicular to the c axis. Three of the title compounds show large powder second harmonic generation (SHG) effects at 2.05 μm, and two of them also exhibit large transparency ranges (1.75 or 0.75 to 25 μm) in the middle-IR region. Significantly, the Sm-member exhibits the strongest SHG response among sulfides to date with intensity approximately 3.8 times that of the benchmark $AgGaS_2$. The band structures, indirect band gap nature, bonding strengths, and lone pair effects around Sb have also been studied by Vienna ab initio simulation package calculations.

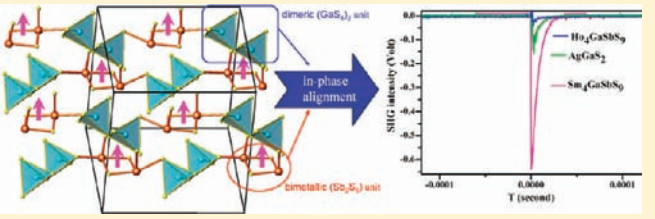

INTRODUCTION

Middle-IR (2−20 μm) nonlinear optical (NLO) materials are suitable in two important atmospheric transparent window bands, i.e., band I (3−5 μm) and band II (8−14 μm), in which they have received increased demands in molecular spectroscopy, atmospheric sensing, communications, and various optoelectronic devices over the past several decades.[1] However, the well-known oxide NLO materials, such as KH_2PO_4 (KDP),[2] $KTiOPO_4$ (KTP),[3] LiB_3O_5 (LBO),[4] β-BaB_2O_4 (BBO),[5] are not suitable in this region because of inadequate optical transparency and relatively low second harmonic generation (SHG efficiency). Chalcogenide semiconductors are more promising in the IR because of their large NLO coefficients and wide transparency, but the number of the available materials is limited. The typical mid-IR benchmark materials are $AgGaS_2$ (SHG coefficient: d_{36}(10.6 μm) = 12 pm/V, transparency: 0.43−13 μm)[1a,6] and $ZnGeP_2$ (d_{36}(10.6 μm) = 69 pm/V, transparency: 0.74−12 μm).[1a,7] However, both of them have drawbacks, such as a low laser damage threshold for the former and the two-photon absorption of 1 μm laser by the latter. Recent great efforts in searching for new mid-IR NLO materials have given rise to the discovery of many new compounds, including $AgGaGeS_4$ (a solid solution with d_{31} (7 μm) = 12 pm/V, transparency: 0.5−11.5 μm),[8] $LiInS_2$ (d_{31}(0.8 μm) = 7.5 pm/V, transparency: 0.41−12 μm),[9] $LiGaS_2$ (d_{31}(0.8 μm) = 5.8 pm/V, transparency: 0.31−11.6 μm),[10] and $BaGa_4S_7$ (d_{33}(2.05 μm) = 12 pm/V, transparency: 0.35−13.7 μm),[11] some of which show NLO properties similar to the benchmark $AgGaS_2$. The new NLO compounds also include some pnicogen-containing compounds with attractive NLO properties, for instance, $AZrPSe_6$,[12] $Cs_5BiP_4Se_{12}$,[13] $Li_{1-x}Na_xAsS_2$,[14] and $NaAsSe_2$.[15] Note that, the strongest SHG signal intensities of these chalcophosphates and chalcoarsonates are found below 1.0 μm. In comparison, the NLO chalcoantimonides are still extremely rare, the two known examples being $AgSbS_3$,[16] established in 1970s with SHG coefficient half that of $AgGaS_2$, and polycationic $[Sb_7S_8Br_2](AlCl_4)_3$, showing a much lower SHG intensity than $AgGaS_2$.[17]

The NCS packing of asymmetric building units usually generates highly polar compounds. In our previous work, we found asymmetric building units, SbS_4 teeter-totter polyhedra (a SbS_3 pyramid with an extra long Sb−S bond) or SbS_5 square pyramids in quaternary compounds. Unfortunately, after linking by the transition-metal polyhedra, for instance, FeS_4 tetrahedra or MnS_6 octahedra, these asymmetric units are evidently always arranged in centrosymmetric structures, $La_4FeSb_2Q_{10}$ (Q = S, Se)[18] and $Ln_2Mn_3Sb_4S_{12}$ (Ln = Pr, Nd, Sm, Gd).[19] In this paper, we extend the exploration to main group elements, resulting in the discovery of seven new NCS compounds of Ln_4GaSbS_9 (Ln = Pr, Nd, Sm, Gd, Tb, Dy, Ho) in which the asymmetric SbS_4 teeter-totter polyhedra are jointed by vertex-sharing dimeric

Received: December 10, 2010
Published: March 03, 2011

   dx.doi.org/10.1021/ja1111095 | *J. Am. Chem. Soc.* 2011, 133, 4617–4624

Table 1. Crystal Data and Structure Refinements for Ln_4GaSbS_9[a]

formula	Pr_4GaSbS_9	Nd_4GaSbS_9	Sm_4GaSbS_9	Gd_4GaSbS_9	Tb_4GaSbS_9	Dy_4GaSbS_9	Ho_4GaSbS_9
fw	1043.65	1056.97	1081.41	1109.01	1115.69	1130.01	1139.73
crystal system	orthorhombic	orthorhombic	orthorhombic	orthorhombic	orthorhombic	orthorhombic	orthorhombic
crystal color	orange yellow	orange yellow	orange yellow	orange yellow	orange yellow	orange yellow	orange yellow
space group	*Aba*2 (no. 41)	*Aba*2 (no. 41)	*Aba*2 (no. 41)	*Aba*2 (no. 41)	*Aba*2 (no. 41)	*Aba*2 (no. 41)	*Aba*2 (no. 41)
a (Å)	13.799(3)	13.759(5)	13.640(3)	13.573(2)	13.530(5)	13.476(2)	13.427(5)
b (Å)	14.187(3)	14.113(5)	13.983(3)	13.896(2)	13.850(5)	13.811(2)	13.756(5)
c (Å)	14.323(3)	14.300(5)	14.166(3)	14.098(2)	14.050(5).	14.011(2)	13.954(5)
V (Å^3)	2804(2)	2777(2)	2702(2)	2659.0(6)	2633(2)	2607.6(5)	2577(2)
D_c (g.cm^{-3})	4.945	5.057	5.317	5.540	5.629	5.757	5.874
μ (mm^{-1})	18.719	19.825	22.387	25.034	26.620	28.105	29.800
GOOF on F^2	1.127	1.228	1.091	1.308	1.044	1.000	1.015
R_1, wR_2 ($I > 2\sigma(I)$) [a]	0.0180, 0.0335	0.0165, 0.0381	0.0367, 0.0857	0.0114, 0.0265	0.0329, 0.0694	0.0255, 0.0509	0.0305, 0.0634
R_1, wR_2 (all data)	0.0204, 0.0417	0.0194, 0.0693	0.0411, 0.1338	0.0128, 0.0596	0.0360, 0.0722	0.0274, 0.0520	0.0322, 0.0645
absolute structure parameter	−0.02(2)	−0.03(2)	0.05(4)	0.03(2)	0.01(2)	0.08(2)	0.06(2)

[a] $R_1 = \Sigma||F_o| - |F_c||/\Sigma|F_o|$, $wR_2 = [\Sigma w(F_o^2 - F_c^2)^2/\Sigma w(F_o^2)^2]^{1/2}$.

GaS_4 tetrahedra that are aligned in-phase in a pseudolayer motif. Significantly, the Sm- and Gd-members exhibit strong SHG effects at 2.05 μm with the intensities about 3.8 and 0.8 times that of benchmark $AgGaS_2$ with large transparency ranges in 1.75−25 and 0.75−25 μm, respectively. These results distinguish Sm_4GaSbS_9 as the strongest SHG response in the middle-IR region among sulfides. The band structures, bond strengths, and lone pair effects around Sb have also been studied by ab initio calculations with the aid of Vienna ab initio simulation package (VASP). The syntheses, crystal structures, electronic structures, and magnetic properties are also reported.

EXPERIMENTAL SECTION

Synthesis. The elements were used as acquired and stored in an argon-filled glovebox (moisture and oxygen levels less than 0.1 ppm), and all manipulations were carried out in the glovebox or under vacuum. Pure elements, purchased from Huhhot Jinrui Rare Earth or Sinopharm Chemical Reagent, with purities of 99.99% or higher, were loaded in the desired stoichiometric ratios in silica crucibles within fused silica jackets and then flame-sealed under high vacuum of 10^{-3} Pa. The reaction mixtures were heated in high-temperature tube furnaces according to the profile described below.

The orange-yellow crystals of the title compounds were obtained from mixtures of Ln, Ga, Sb, and S (in ratios of Ln/Ga/Sb/S = 8:1:1:15) after being heated at 950 °C. After trying many different conditions, the optimal conditions to synthesize most of the members involved heating of stoichiometry mixtures to 950 °C (at a rate of 26.5 °C/h), a dwell period at this temperature for 5 days, and then slowly cooling to 300 °C (at a rate of 5 °C/h), at which point the furnace was switched off. The orange-yellow products are stable in air at room temperature for long periods of time (more than six months). For the members of Ln = Sm, Gd, Tb, Dy, Ho, pure phase products were obtained from the stoichiometric mixture of elements following the heating profile described above; their X-ray powder diffraction (XRD) patterns are shown in Figure S1c−g, Supporting Information. For Ln = Pr and Nd, mixtures of the target quaternary compounds together with ∼50% of binary byproducts of Ga_2S_3 and Ln_2S_3 were obtained (Figure S1a−b, Supporting Information). For Ln = La and Eu, the same attempts did not yield the same quaternary phases, and only ternary or binaries, such as $EuGa_2S_4$, La_2S_3, Ga_2S_3, and Sb_2S_3 were found. The possible reasons are that europium is susceptible to adopt the formal oxidation state of +2 in a chalcogenide system, while the binary La_2S_3 phases are more stable.

Table 2. Atomic Coordinates and Equivalent Isotropic Displacement Parameters of Sm_4GaSbS_9

atom	oxidation state	Wyckoff	x	y	z	U(eq)
Sm1	+3	8*b*	0.6855(1)	0.6090(1)	0.9823(1)	0.010(1)
Sm2	+3	8*b*	0.8990(1)	0.8278(1)	0.9942(1)	0.010(1)
Sm3	+3	8*b*	0.8189(1)	0.8345(1)	0.7099(1)	0.011(1)
Sm4	+3	8*b*	0.6038(1)	0.8881(1)	0.9384(1)	0.012(1)
Sb	+3	8*b*	0.8869(1)	0.5790(1)	0.7527(1)	0.016(1)
Ga	+3	8*b*	0.5925(2)	0.6050(2)	0.7205(2)	0.010(1)
S1	−2	8*b*	0.9002(4)	0.5891(4)	0.9248(4)	0.010(1)
S2	−2	8*b*	0.5819(4)	0.9067(4)	0.7396(4)	0.013(1)
S3	−2	8*b*	0.6982(4)	0.5122(3)	0.8067(4)	0.011(1)
S4	−2	8*b*	0.6901(4)	0.6967(4)	0.6257(4)	0.009(1)
S5	−2	4*a*	1.0000	1.0000	0.6316(6)	0.023(2)
S6	−2	8*b*	0.9946(4)	0.8050(3)	0.8148(4)	0.014(1)
S7	−2	8*b*	0.9320(4)	0.7473(3)	0.5679(4)	0.010(1)
S8	−2	8*b*	0.7498(4)	0.9429(3)	0.5624(4	0.010(1)
S9	−2	4*a*	1.0000	1.0000	1.0000(6)	0.014(2)
S10	−2	8*b*	0.7464(4)	0.7656(3)	0.8768(4)	0.012(1)

Crystal Structure Determinations. All data collections were performed at 293 K on a Rigaku Saturn70 CCD or Mercury CCD automatic diffractometer equipped with graphite-monochromated Mo Kα radiation (λ = 0.71073 Å). The orange-yellow crystals were mounted on glass fibers for the structure determination. The data were corrected for Lorentz and polarization factors. Absorption corrections were performed by the multiscan method.[20] All structures were solved by direct methods and refined by the full-matrix least-squares fitting on F^2 by SHELX-97.[21]

Systematic absence statistics for each data set suggested that *Aba*2 (noncentrosymmetric) or *Cmca* (centrosymmetric) were the only two candidate space groups, but the significantly better refinement results for *Aba*2 suggested that it was the correct space group for all title compounds. Additionally, the strong SHG effect from Sm_4GaSbS_9 confirmed the assignment to the noncentrosymmetric space group. Crystallographic data and structural refinement details were summarized in Tables 1−2 and Table S1, Supporting Information.

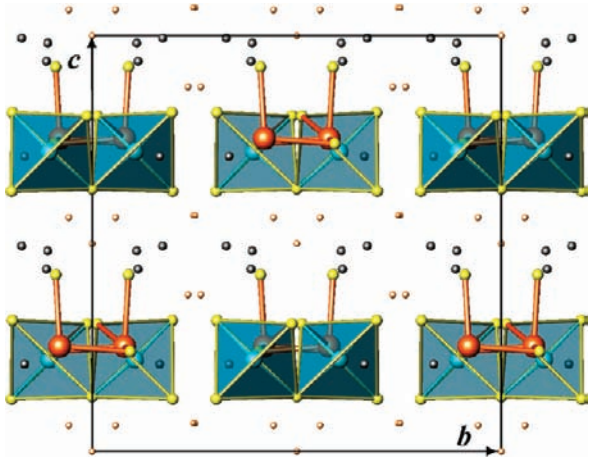

Figure 1. Structure of orthorhombic Sm_4GaSbS_9 viewed down *a* axis with unit cell marked. The Sm−S bonds are omitted for the sake of clarity. Blue: Ga; orange: Sb; yellow: S; pink: interlayer S7−S10; black: Sm; and blue tetrahedron: GaS_4 tetrahedron. Anionic $\{[(Ga_2S_6)(Sb_2S_5)]^{10-}\}_\infty$ chains are arranged in a pseudolayer motif perpendicular to *c* axis.

X-ray Powder Diffraction. The XRD patterns were collected on a Rigaku DMAX 2500 diffractometer at 40 kV and 100 mA for Cu Kα radiation (λ = 1.5406 Å) with a scan step of 0.05° at ambient temperature ($2\theta_{max}$ = 80°).

Magnetic Susceptibility. The direct current magnetic susceptibility measurements were performed on a Quantum Design MPMS-XL magnetometer for the Ln_4GaSbS_9 (Ln = Sm, Gd, Tb, Dy) in the temperature range of 2−300 K. The pure polycrystalline samples were ground and loaded into gelatin capsules. The data were corrected for the susceptibility of the containers and for the diamagnetic contributions from the ion cores.

UV−Vis, Near IR, and IR Spectroscopies. The optical diffuse reflectance spectra of powdered samples were measured at room temperature using a Perkin-Elmer Lambda 900 UV−vis spectrophotometer equipped with an integrating sphere attachment and $BaSO_4$ as a reference over the range of 0.19−2.5 μm. The absorption spectrum was calculated from the reflection spectrum via the Kubelka−Munk function: $\alpha/S = (1-R)^2/2R$, in which α is the absorption coefficient, *S* is the scattering coefficient, and *R* is the reflectance.[22] The IR data were measured by a Nicolet Magana 750 FT-IR spectrophotometer in the range of 2.5−25 μm. Polycrystalline samples were ground with KBr and pressed into transparent pellets for the IR spectra measurement.

Second Harmonic Generation Measurements. The SHG responses on powdered samples were measured by using the Kurtz and Perry method with 2.05 μm Q-switch laser.[23] The Sm_4GaSbS_9 and Gd_4GaSbS_9 samples were ground and sieved by means of a series of mesh sizes in the range of 30−46, 46−74, 74−106, 106−150, and 150−210 μm, respectively, whereas Tb_4GaSbS_9 and Ho_4GaSbS_9 were sieved with 46−74 μm. Powdered $AgGaS_2$ was used as a reference, sieved with the same size range.

Electronic Structure Calculations. The electronic band structure of the compounds Ln_4GaSbS_9 (Ln = Pr, Nd, Sm, Gd, Tb, Dy, Ho) was calculated by VASP.[24] The generalized gradient approximation (GGA)[25] was chosen as the exchange−correlation functional, and a plane wave basis with the projector augmented wave (PAW) potentials was used.[26] The plane wave cutoff energy of 310 eV and the threshold of 10^{-5} eV were set for the self-consistent field convergence of the total electronic energy. The 4f electrons of Ln were treated as core electrons, and the valence electrons of the elements included Sb, $5s^25p^3$; Ga, $4s^24p^1$; and S, $3s^23p^4$. The *k* integration over the Brillouin zone was performed by the tetrahedron method[27] using a 6 × 6 × 4 Monkhorst−Pack mesh, and the Fermi level (E_f = 0 eV) was selected as the reference of the energy.

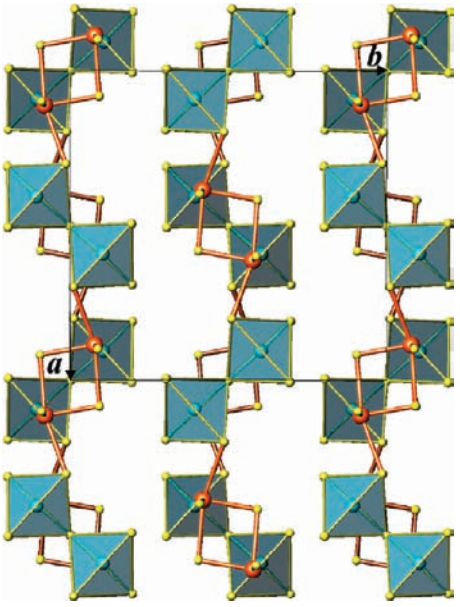

Figure 2. The noncentrosymmetric packing of the $\{[(Ga_2S_6)(Sb_2S_5)]^{10-}\}_\infty$ chains in Sm_4GaSbS_9 viewed down the *c* axis. Blue: Ga; orange: Sb; and yellow: S. Chains with darken color are at 0.5 < *c* < 1.0, and chains with bright color are at 0 < *c* < 0.5. The interlayer Sm and S ions are omitted for the sake of clarity.

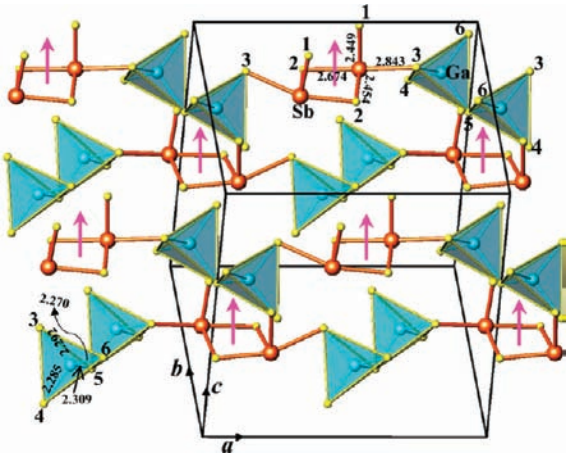

Figure 3. A pseudolayer of separated infinite $\{[(Ga_2S_6)(Sb_2S_5)]^{10-}\}_\infty$ chains at 0.5 < *c* < 1.0. The Sb is asymmetrically coordinated by one S1, two S2, and one μ_2-S3 atoms, and the Ga-centered coordination sphere is a nearly ideal tetrahedron formed by μ_2-S3, S4, S5, and S6. The Ga−S and Sb−S bond lengths are in Å. The connectivity between dimeric $(GaS_4)_2$ tetrahedra and asymmetric bimetallic (Sb_2S_5) units is shown. The pink arrows show the in-phase alignment of such chains.

RESULTS AND DISCUSSION

Crystal Structure. The title compounds Ln_4GaSbS_9 (Ln = Pr, Nd, Sm, Gd, Tb, Dy, Ho) crystallize in orthorhombic NCS space group, *Aba*2 (no. 41). The structure features infinite single anionic chains of $\{[(Ga_2S_6)(Sb_2S_5)]^{10-}\}_\infty$ built up of bimetallic asymmetric (Sb_2S_5) units linked with corner-sharing dimeric

dx.doi.org/10.1021/ja1111095 |*J. Am. Chem. Soc.* 2011, 133, 4617–4624

$(GaS_4)_2$ tetrahedra (Figure 1). These infinite chains are parallel and separated by Ln^{3+} cations and interlayer S^{2-} anions (S7, S8, S9, and S10).

Figure 1 shows the packing of these single infinite chains of $\{[(Ga_2S_6)(Sb_2S_5)]^{10-}\}_\infty$ arranged in a NCS pseudolayer motif perpendicular to the *c* axis. Another view down the *c* axis showing the overlay of two such pseudolayers is in Figure 2. The *c* glide plan at (1/4, *y*, *z*) relates the chains on the lower layer ($0 < c < 0.5$) to those on the upper layer ($0.5 < c < 1.0$). This NCS packing of the chains generates the in-phase alignment of the dipoles of both (Sb_2S_5) and $(GaS_4)_2$ units, as indicated in Figure 3. Each chain is built up of bimetallic polar (Sb_2S_5) units linked with dimeric polar $(GaS_4)_2$ tetrahedra via μ_2-S3 atoms (Figure 3). The GaS_4 tetrahedra are dimerized via linking vertex (S5), while the (SbS_4) units via S2−S2 edge. The small distortion of GaS_4 tetrahedron is indicated by the small deviations of both the Ga−S bond lengths (2.270(6)−2.309(6) Å) and the S−Ga−S angles (105.34−112.19°). These data are consistent with those observed in $AgGaS_2$ (2.276(2) Å; 108.68−111.08°);[28] $BaGa_4S_7$ (2.229(2)−2.338(2) Å; 102.86−127.25°),[11] and $Li_2Ga_2GeS_6$ (2.219(3)−2.233(3) Å; 101.51−114.65°).[29]

On the contrary, the distortion of the Sb-centered local coordination sphere is remarkable. The Sb^{3+} cation is four-fold-coordinated in a teeter-totter-shaped geometry (Figure 3) constructed by a long Sb−S3 bond and three short length Sb−S bonds. The S3−Sb−S2 bond angle is 160.68° indicating a nearly linear bond, and other S−Sb−S angles range from 79.53 to 96.83°. These data are comparable with those found in other antimonides, for instance, $La_4FeSb_2Q_{10}$ (2.458(1)−2.918(2) Å; 79.08−156.02°);[18] $La_7Sb_9S_{24}$ (2.428(1)−2.997(2) Å; 73.85−171.50°),[30] and $Eu_6Sb_6S_{17}$ (2.416(3)−3.106(3) Å; 83.14−178.28°).[31] Such a distorted SbS_4 environment is different from the common three-coordinated pyramidal coordination sphere for Sb (III) as observed in $Sr_6Sb_6S_{17}$,[32] $CsAgSb_4S_7$,[33] or $Cs_3Ag_2Sb_3S_8$.[34] The teeter-totter-shaped polar SbS_4 geometry has also been seen in $La_4FeSb_2Q_{10}$ (Q = S, Se), in which the SbS_4 units have been linked in a different symmetric layered motif.[18] In comparison, the asymmetric alignment of the SbS_4 building unit in the title compound (Figure 3) is novel and remarkable and gives rise to the strong SHG response.

The Sm^{3+} cations and interlayer S^{2-} anions (S7, S8, S9 and S10) occur between the infinite single anionic chains of $\{[(Ga_2S_6)(Sb_2S_5)]^{10-}\}_\infty$. The Sm atoms are coordinated with seven or six S atoms in common environments, such as seven-coordinated monocapped octahedra for Sm1 and distorted six-coordinated octahedra for Sm2, Sm3, and Sm4 (Figure S2, Supporting Information). All Sm−S bond lengths are normal, varying over 2.729(5)−3.052(6) Å (Table S2, Supporting Information). The size of the rare-earth metal cation does not affect the packing of the anionic chains in the title compounds, Ln_4GaSbS_9 (Ln = Pr, Nd, Sm, Gd, Tb, Dy, Ho), only a reduction of the unit cell parameters on going from Pr to Ho as their radii decrease (Table 1). Such a reduction is known as lanthanide contraction. Nevertheless, the rare-earth metal cations do affect the band gap via participation in the bottom of the conduction band. Although the interlayer sulfur atoms are not involved in the construction of the functional substructure, the linear $\{[(Ga_2S_6)(Sb_2S_5)]^{10-}\}_\infty$ chain of the SHG response, they contribute significantly at the top of the valence band, as discussed below, and therefore are involved in the band gap transition.

Magnetic Properties. The inverse magnetic susceptibility data over the entire temperature range for the Gd-, Tb-, and Dy-members (Figure 4a) can be fit to the Curie−Weiss law, $\chi_M = C/(T-\theta)$. The Curie constants are $C = 32, 47$, and 56 $cm^3\ mol^{-1}K$, and the Weiss constants are $\theta = -7.3$, -6.9, and -5.8 K, respectively. The effective magnetic moments, obtained from the equation $\mu_{eff} = (8C)^{1/2}\ \mu_B$,[35] are 8.0 μ_B/Gd, 9.7 μ_B/Tb, and 10.6 μ_B/Dy, which agree well with the theoretical values for the isolated ground-state Ln^{3+} ions (7.9, 9.7, and 10.6 μ_B, respectively) obtained from the equation $\mu_{eff} = g[J(J+1)]^{1/2}$.[36,37] The negative sign of θ indicates a relatively weak local antiferromagnetic interaction between Ln^{3+} ions (Figure 4a). The inverse magnetic susceptibility for Sm_4GaSbS_9 does not follow the Curie−Weiss law (Figure 4b) and is typical for Sm^{3+}-containing compounds, where spin−orbit coupling splits the ^6H ground term for Sm^{3+}, leading to a temperature dependence of the effective moment from the 4f electrons. In general, these results are comparable to those found for $Ln_6Zn_{1+x}Sb_{14}$,[38] $CsLnCdTe_3$,[39] and $ZnLn_6Si_2S_{14}$,[40] which also show the antiferromagnetic ordering between the isolated Ln^{3+} ions.

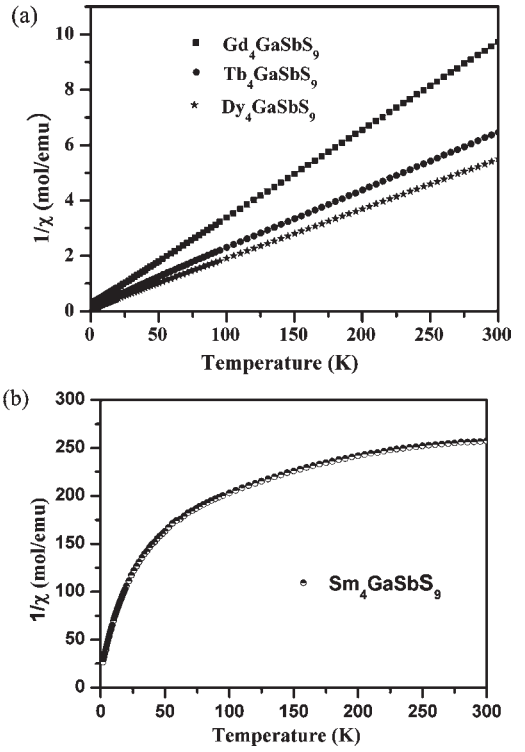

Figure 4. Plots of the inverse molar susceptibility $(1/\chi)$ versus *T* for Ln_4GaSbS_9 (Ln = Gd, Tb, Dy, Sm).

Optical Properties. The powder SHG properties of the title compounds were measured. The plots of particle size versus SHG intensity are shown in Figure 5a indicate that Sm_4GaSbS_9 and Gd_4GaSbS_9 are not type-I phase matchable[41] at 2.05 μm. Relative powder SHG intensities of Sm_4GaSbS_9, Gd_4GaSbS_9, and Ho_4GaSbS_9 are about 3.8, 0.8, and 0.25 times that of $AgGaS_2$ in the same particle size of 46−74 μm (Figure 5b), whereas the polycrystalline Tb_4GaSbS_9 phase yields a very weak SHG response. And the SHG responses of the Pr-, Nd-, Dy-compounds are nondetectable. It is interesting that although the identity of the rare-earth metal cation does not affect the crystal structure, it affects the intensity of the SHG response. The essential reasons are currently under study and will be published in a separated article. The powder SHG response of Sm_4GaSbS_9 is the largest among sulfides in middle-IR region at 2.05 μm.

dx.doi.org/10.1021/ja1111095 |J. Am. Chem. Soc. 2011, 133, 4617–4624

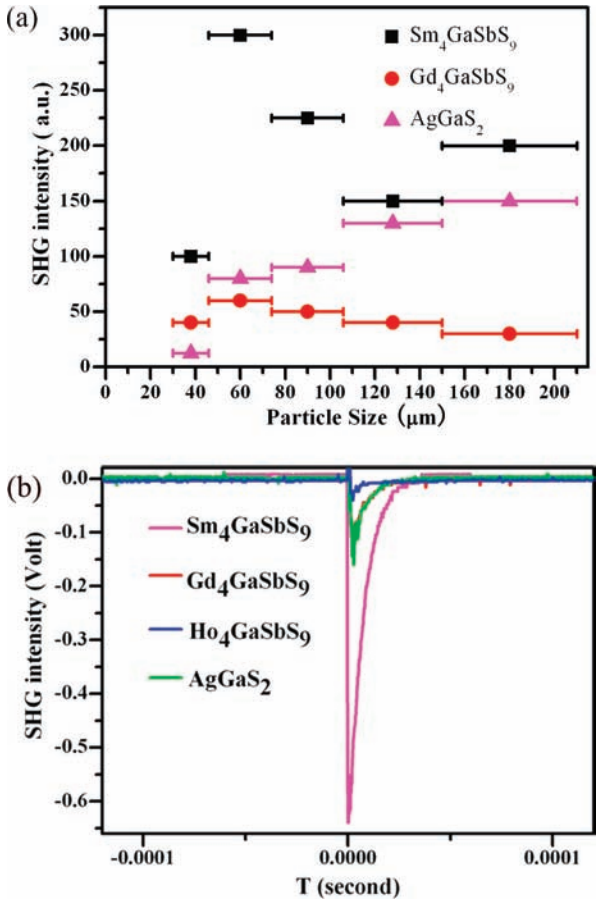

Figure 5. (a) Phase-matching curves, i.e., particle size versus SHG response, for Sm_4GaSbS_9 and Gd_4GaSbS_9. That of the reference (benchmark $AgGaS_2$) is also shown. (b) Oscilloscope traces of SHG signals of Sm_4GaSbS_9, Gd_4GaSbS_9, Ho_4GaSbS_9, and $AgGaS_2$ (reference).

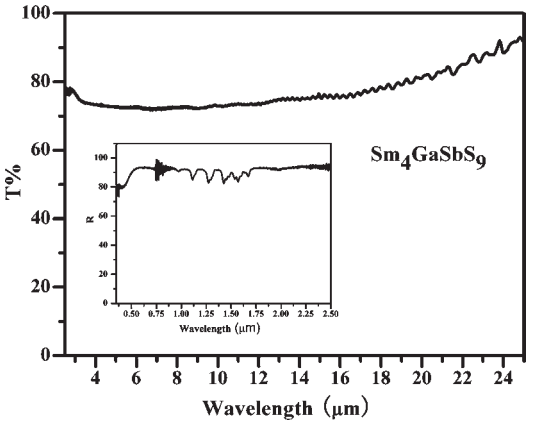

Figure 6. Reflection spectrum (inset panel) and FT-IR spectrum of Sm_4GaSbS_9. The diffuse reflection spectrum of Sm_4GaSbS_9 is shown in Figure S3a, Supporting Information.

The SHG intensities of some sulfides are weaker than this value, such as $ZnY_6Si_2S_{14}$ (twice that of KTP at 2.05 μm)[40] and $BaGa_4S_7$ (1.4 times that of $LiGaS_2$ at 2.05 μm; d_{33} (2.05 μm) = 12 pm/V).[11]

The band gaps were measured to be 2.23, 2.41, 2.44, and 2.58 eV for Sm-, Gd-, Tb-, and Dy-compounds, respectively (Figure S3, Supporting Information), which are consistent with their orange-yellow colors and close to those found in other IR NLO crystals, such as $ZnY_6Si_2S_{14}$[40] (2.38 eV), $ZnGeP_2$[42] (2.0 eV), and $AgGaS_2$[43] (2.62 eV). Since the as-synthesized Pr- and Nd-compounds contained binary impurities, we did not measure their band gaps. For the Ho-compound, the acceptable diffuse reflectance spectrum and IR data cannot be obtained. Sm_4GaSbS_9 exhibits characteristic sharp absorption peaks at 976, 1115, 1274, 1428, 1574, and 1670 nm (Figure S3a, Supporting Information), corresponding to f−f transitions of Sm^{3+} ions.[44] Some of the title compounds exhibit high transparency over a broad range: Sm: 1.75−25 μm (Figure 6); Gd: 0.75−25 μm (Figure S4a, Supporting Information); and Tb: 2.5−25 μm (Figure S4b, Supporting Information). These ranges are larger than those of

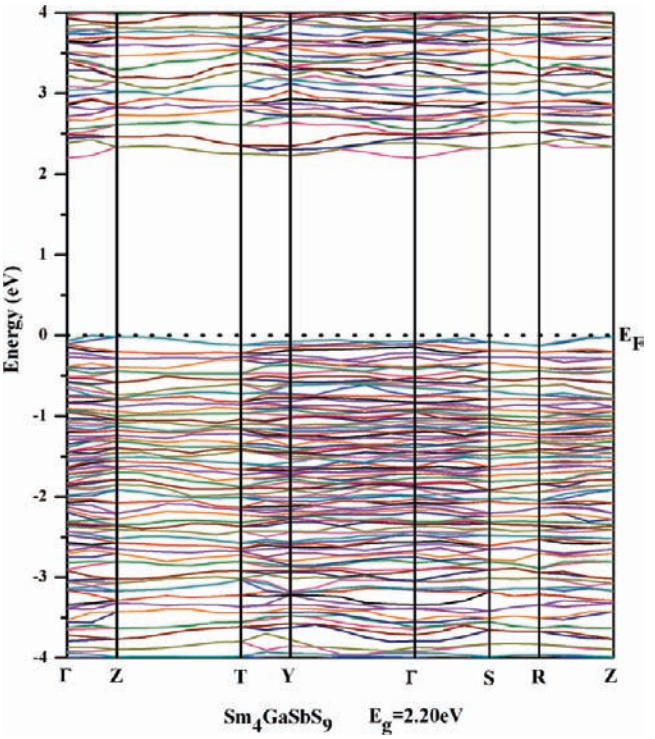

Figure 7. Calculated band structure of Sm_4GaSbS_9, Γ (0,0,0), Y (1/2, 1/2, 0), Z (0, 0, 1/2), T (1/2, 1/2, 1/2), S (0, 1/2, 0), and R (0, 1/2, 1/2).

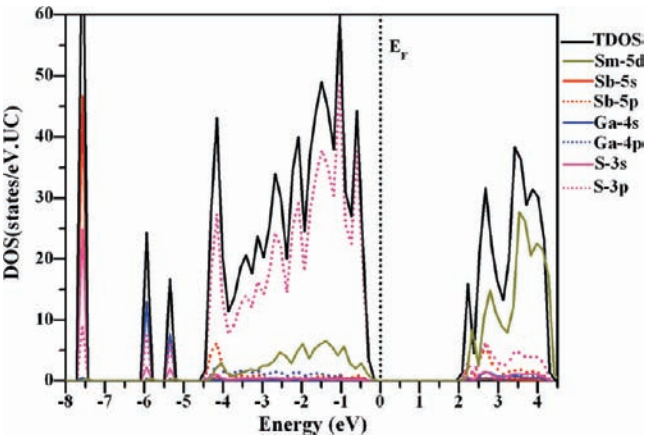

Figure 8. Total and partial DOS for Sm_4GaSbS_9.

dx.doi.org/10.1021/ja1111095 |J. Am. Chem. Soc. 2011, 133, 4617–4624

related compounds, such as, $AgGaS_2$ (0.43−13 μm),[1a] $ZnGeP_2$ (0.74−12 μm),[1a] and $ZnY_6Si_2S_{14}$(2.5−14.3 μm).[40]

Theories. The band structures for Ln_4GaSbS_9 have been calculated; those of the selected example, Sm_4GaSbS_9, are shown in Figure 7 and others in Figure S5, Supporting Information. The valence band (VB) maximum and conduction band (CB) minimum, as shown in Figure 7, are not located at the same *k*-point indicating an indirect gap semiconductor nature of Sm_4GaSbS_9. The calculated band gap of Sm_4GaSbS_9 is 2.20 eV, consistent with the experimental value (2.23 eV) derived from the UV−vis diffuse reflection spectrum. The component of each band studied by a projected density-of-states analysis (PDOSs) is shown in Figure 8. For instance, VB spanning −8 to −7 eV comes predominantly from Sb-5s and S-3s states and a minor S-3p state. The VB ranging from −5 eV to E_F mainly consists of S-3p states with a small contribution from Sm-5d and neglectable Sb-5p, Sb-5s, and Ga-4p states. The bottom of the conduction band (CB) is primarily dominated by Sm-5d, with minor contribution from Sb-5p and S-3p states. Thus the fundamental band edge excitation is believed to originate from transitions involving the filled primarily sulfur-based p states in VB and the empty Sm-d states in CB.

The electron localization function (ELF)[45] calculation was performed to visualize the stereochemically active lone pair and the nature of the chemical bond in Sm_4GaSbS_9. The isosurface around Sb associated with a given ELF value (η = 0.64) in Figure 9 clearly illustrates that the four Sb−S bonds with different lengths indeed possess different bond strengths. The longer the bond length, the weaker is the bond interaction. The orders of the orbital overlapping are Sb1−S2 (2.454 Å) ≈ Sb1−S1 (2.449 Å) > Sb1−S2 (2.674 Å) ≫ Sb1−S3 (2.843 Å). As shown in Figure 10, with a given ELF value (η = 0.64), a lobelike isosurface near each Sb^{3+} ion is observed, which can be considered as the stereochemically active lone pairs. On the other band, there is no obvious lobe-like isosurface near each Ga^{3+} ion with the given ELF value as expected.

As there are four structurally different types of S ions in Sm_4GaSbS_9; the DOS of each type of S ion are compared in Figure 11. These four types of S are type I: S1 and S2, coordinated to the Sb center; type II: μ_2-S3, the bridging atoms that connect dimeric $(GaS_4)_2$ tetrahedra and bimetallic asymmetric (Sb_2S_5) units; type III: S4−S6, bonded to the Ga center; and type IV: S7−S10, the interlayer sulfur ions that are only coordinated to Sm (detailed in Figure S2, Supporting Information). The bonding interactions between gallium and sulfur atoms (μ_2-S3, S4, S5, and S6) are strong, and the hybridization between them is strong as shown in Figure 11. However, the interaction between μ_2-S3 and Sb is very weak, which is confirmed by the plot of ELF in Figure 9. These results indicate that the $\{[(Ga_2S_6)(Sb_2S_5)]^{10-}\}_\infty$ chain is actually a chain-like array of discrete bimetallic asymmetric (Sb_2S_5) units and dimeric $(GaS_4)_2$ tetrahedra. The interactions between the interlayer S ions (S7−S10) and Sm ions are indicated

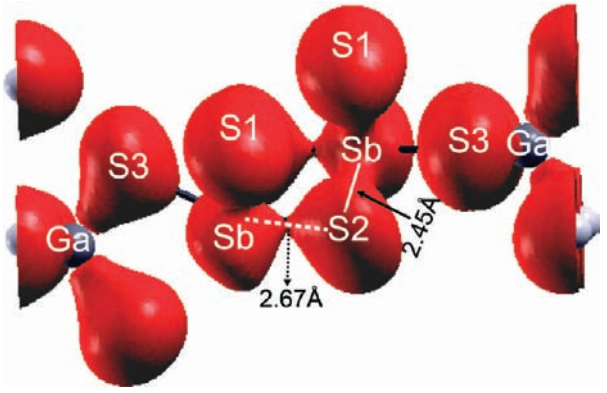

Figure 9. Isosurface plot of the ELF associated with a given ELF value (η = 0.64) for Sm_4GaSbS_9. For the sake of clarity, only those around a (Sb_2S_5) unit of a single $\{[(Ga_2S_6)(Sb_2S_5)]^{10-}\}_\infty$ chain are shown. The two different Sb−S2 bond lengths are denoted.

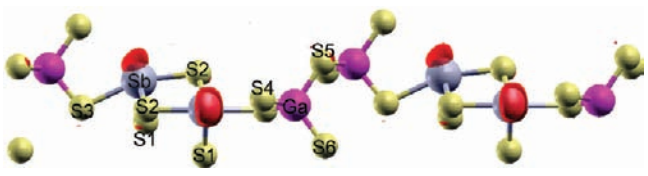

Figure 10. Isosurface plot of the ELF associated with a given ELF value (η = 0.93) for Sm_4GaSbS_9. For comparison, only those around two (Sb_2S_5) units of a single $\{[(Ga_2S_6)(Sb_2S_5)]^{10-}\}_\infty$ chain are shown. An asymmetric lobe-like isosurface (red) near each Sb^{3+} center is observed; dissimilarly, an asymmetric isosurface around Ga^{3+} center is not obvious at the given ELF value.

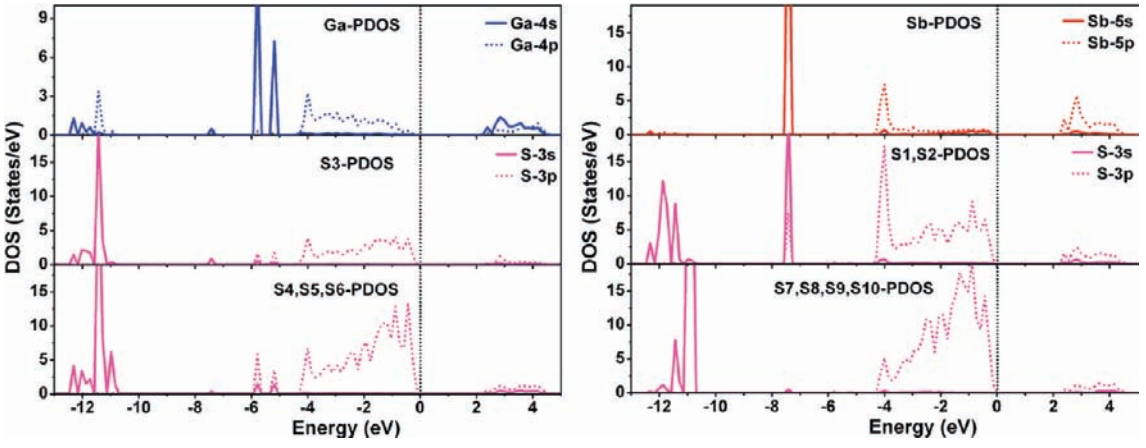

Figure 11. The projected DOS of Ga, Sb, and four different types of S ions of Sm_4GaSbS_9: S7−S10 are the interlayer sulfur ions that are only coordinated to Sm ions; S4−S6 are bonded to Ga; μ_2-S3 is the bringing ions between the dimeric $(GaS_4)_2$ tetrahedra and the bimetallic asymmetric (Sb_2S_5) units, and S1 and S2 are bonded to Sb.

dx.doi.org/10.1021/ja1111095 |*J. Am. Chem. Soc.* 2011, 133, 4617–4624

by the diffuse PDOS of S7−S10 from −4 to 0 eV. And these interlayer S ions contribute to the band gap transition as much as other sulfur atoms forming the $\{[(Ga_2S_6)(Sb_2S_5)]^{10-}\}_\infty$ chains.

The contributions of Sb-5s, Sb-5p, and S-3p states to the electronic structure have also been examined according to the ratios of the integrated PDOSs (IPDOSs) in the two crucial regions in the VB, that is, **region-I**, between −7.7 and −7.4 eV, and **region-II**, from −4.5 to 0 eV, as indicated in Figure 8. In **region-I**, the IPDOS are 87.6% Sb-5s states (exhibiting symmetric s orbital character) and negligible Sb-5p states, whereas in **region-II**, the IPDOS are 93.1% of S-3p states and 4.3% of Sb-5p states. Note that regardless of its small IPDOS ratio, about 12% of the Sb-5s states diffuse in **region-II.** Therefore, the formation of the stereochemically active lone pair on Sb is driven by the Sb−S bonding interactions between sulfur-3p states, antimony-5p states, and (minor) antimony-5s states. Such results are similar to those found in other systems that show lone pair effects, PbO and $Pb_2B_5O_9I$, in which the formation of the stereochemically active lone pairs on Pb^{2+} is also driven by the $Pb^{2+}-O^{2-}$ bonding interactions, instead of the classical view of hybridization of lead 6s with 6p orbitals.[46]

CONCLUSION

In summary, new noncentrosymmetric rare-earth gallium thioantimonates, Ln_4GaSbS_9, were discovered and characterized. These compounds show a unique polar structure in which the asymmetric building units, bimetallic polar (Sb_2S_5) units, and dimeric $(GaS_4)_2$ tetrahedra are aligned in-phase. Although the size of the interlayer rare-earth cation does not affect the packing of the structure, the identity of the rare-earth metal ions affect the band gap transition and the SHG response. The VASP calculations visualize stereochemically active lone pair on Sb and reveal the driving force of the formation of such lone pairs is the Sb−S bonding interaction. These compounds are indirect semiconductors with band gaps of 2.2−2.6 eV. Remarkable, the Sm-member exhibits the strongest powder SHG effects among sulfides to date at 2.05 μm with intensity about 3.8 times that of benchmark $AgGaS_2$ and a good transparency in a wide middle-IR range, 1.75−25 μm. These primary data suggest that Sm_4GaSbS_9 may be potential middle-IR NLO material. Further studies are ongoing.

ASSOCIATED CONTENT

Supporting Information. The cif data and additional tables and figures. This material is available free of charge via the Internet at http://pubs.acs.org.

AUTHOR INFORMATION

Corresponding Author
chenl@fjirsm.ac.cn

ACKNOWLEDGMENT

This research was supported by the National Natural Science Foundation of China under projects (90922021, 20773130, 20733003, 20803080, and 20973175), the "Knowledge Innovation Program of the Chinese Academy of Sciences" (KJCX2-YW-H20 and CXJJ-11-M71). We thank Prof. Ning Ye and Dr. Xin-Song Lin at FJIRSM for help with the SHG measurements.

REFERENCES

(1) (a) Dmitriev, V. G.; Gurzadyan, G. G.; Nikogosyan, D. N. *Handbook of Nonlinear Optical Crystals*, Springer: New York, 1999. (b) Ebrahim-Zadeh, M.; Sorokina, I. T. ; *NATO Science for Peace and Security Series B: Physics and Biophysics*; Springer: New York, 2007. (c) Nikogosyan, D. N. *Nonlinear optical crystals: a complete survey*; Springer-Science: New York, 2005.

(2) Chen, C. T.; Wu, B. C.; Jiang, A. D.; You, G. M. *Sci. Sin., Ser. B (Engl. Ed.)* **1985**, *18*, 235.

(3) (a) Jeggo, C. R.; Boyd, G. D. *J. Appl. Phys.* **1970**, *41*, 2741. (b) Levine, B. F. *Phys. Rev. B.* **1972**, *7*, 2600. (c) Bergman, J. G.; Crane, G. R. *J. Solid State Chem.* **1975**, *12*, 172.

(4) (a) Konig, H.; Hoppe, R. *Z. Anorg. Allg. Chem.* **1978**, *439*, 71. (b) Xia, Y. N.; Chen, C. T.; Tang, D. Y.; Wu, B. C. *Adv. Mater.* **1995**, *7*, 79.

(5) (a) Froehlich, R. Z. *Kristallogr.* **1984**, *168*, 109. (b) Chen, C. T.; Wu, B. C.; Jiang, A. D.; You, G. M. *Sci. China, Ser. B: Chem.* **1985**, *28*, 235. (c) Xiao, R. F.; Ng., L. C.; Yu, L. C.; Wong, G. K. L. *Appl. Phy. Lett.* **1995**, *67*, 305. (d) Nikogosyan, D. N. *Appl. Phys. A: Mater. Sci. Process.* **1991**, *52*, 359. (e) Kouta, H.; Kuwano, Y.; Ito, K.; Marumo, F. *J. Cryst. Growth* **1991**, *114*, 676.

(6) Harasaki, A.; Kato, K. *Jpn. J. Appl. Phys.* **1997**, *36*, 700.

(7) Giles, N. C.; Bai, L. H.; Chirila, M. M.; Garces, N. Y.; Stevens, K. T.; Schunemann, P. G.; Setzler, S. D.; Pollak, T. M. *J. Appl. Phys.* **2003**, *93*, 8975.

(8) Petrov, V.; Badikov, V.; Shevyrdyaeva, G.; Panyutin, V.; Chizhikov, V. *Opt. Mater.* **2004**, *26*, 217.

(9) Isaenko, L.; Vasilyeva, I.; Merkulov, A.; Yelisseyev, A.; Lobanov, S. *J. Cryst. Growth* **2005**, *275*, 217.

(10) Isaenko, L.; Yelisseyev, A.; Lobanov, S.; Krinitsin, P.; Petrov, V.; Zondy, J. J. *J. Non-Cryst. Solids* **2006**, *352*, 2439.

(11) Lin, X. S.; Zhang, G.; Ye, N. *Cryst. Growth Des.* **2009**, *9*, 1186.

(12) Banerjee, S.; Malliakas, C. D.; Jang, J. I.; Ketterson, J. B.; Kantzidis, M. G. *J. Am. Chem. Soc.* **2008**, *130*, 12270.

(13) Chung, I.; Song, J. H.; Jang, J. I.; Freeman, A. J.; Ketterson, J. B. *J. Am. Chem. Soc.* **2009**, *131*, 2647.

(14) Bera, T. K.; Song, J. H.; Freeman, A. J.; Jang, J. I.; Ketterson, J. B.; Kantzidis, M. G. *Angew. Chem., Int. Ed.* **2008**, *47*, 1.

(15) Bera, T. K.; Jang, J. I.; Song, J. H.; Malliakas, C. D.; Freeman, A. J.; Ketterson, J. B.; Kanatzidis, M. G. *J. Am. Chem. Soc.* **2010**, *132*, 3484.

(16) Gandrud, W. B.; Boyd, G. D.; Mcfee, J. H. N. *Appl. Phys. Lett.* **1970**, *16*, 59.

(17) Zhang, Q; Chung, I.; Jang, J. I.; Ketterson, J. B.; Kanatzidis, M. G. *J. Am. Chem. Soc.* **2009**, *131*, 9896.

(18) Zhao, H. J.; Li, L. H.; Wu, L. M.; Chen, L. *Inorg. Chem.* **2009**, *48*, 11518.

(19) Zhao, H. J.; Li, L. H.; Wu, L. M.; Chen, L. *Inorg. Chem.* **2010**, *49*, 5811.

(20) *CrystalClear*, version 1.3.5; Rigaku Corp.: The Woodlands, TX, 1999.

(21) Sheldrick, G. M. *SHELXTL*, version 5.1; Bruker-AXS: Madison, WI, 1998.

(22) Kortüm, G. *Reflectance Spectroscopy*; Springer-Verlag: New York, 1969.

(23) Kurtz, S. K.; Perry, T. T. *J. Appl. Phys.* **1968**, *39*, 3798.

(24) (a) Kresse, G.; Furthmüller, J. *Comput. Mater. Sci.* **1996**, 15. (b) Kresse, G.; Furthmüller, J. *Phys. Rev. B: Condens. Matter Mater. Phys.* **1996**, *54*, 11169.

(25) Perdew, J. P.; Wang, Y. *Phys. Rev. B: Condens. Matter Mater. Phys.* **1992**, *45*, 13244.

(26) (a) Kresse, G.; Joubert, D. *Phys. Rev. B: Condens. Matter Mater. Phys.* **1999**, *59*, 1758. (b) BlÖchl, P. E. *Phys. Rev.* **1994**, *B50*, 17953.

(27) BlÖchl, P. E.; Jepsen, O.; Andersen, O. K. *Phys. Rev. B: Condens. Matter Mater. Phys.* **1994**, *49*, 16223.

(28) Abrahams, S. C.; Bernstei, J. I. *J. Chem. Phys.* **1973**, *59*, 1625.

(29) Kim, Y.; Seo, I. S.; Martin, S. W.; Baek, J.; Halasyamani, P. S.; Arumugam, N.; Steinfink, H. *Chem. Mater.* **2008**, *20*, 6048.

(30) Assoud, A.; Kleinke, K. M.; Kleinke., H. *Chem. Mater.* **2006**, *18*, 1041.
(31) Jin, G. B; Well, D. M.; Crerar, S. J.; Shehee, T. C.; Mar, A.; Albrecht-Schmitt, T. E. *Acta Crystallogr., Sect. E: Struct. Rep. Online* **2005**, *61*, 1116.
(32) Choi, K. S.; Kanatzidis, M. G. *Inorg. Chem.* **2000**, *39*, 5655.
(33) Huang, F. Q.; Ibers, J. A. *J. Solid State Chem.* **2005**, *178*, 212.
(34) Wood, P. T.; Schimek, G. L.; Kolis, J. W. *Chem. Mater.* **1996**, *8*, 721.
(35) O'Connor, C. J. *Prog. Inorg. Chem.* **1982**, *29*, 203.
(36) Kahn, O. *Molecular Magnetism*; VCH Publishers: New York, 1993.
(37) van Vleck, J. H. *The Theory of Electric and Magnetic Susceptibilities*; Oxford University Press: Oxford, 1932.
(38) Liu, Y.; Chen, L.; Li, L. H.; Wu, L. M.; Zelinska, O. Y.; Mar, A. *Inorg. Chem.* **2008**, *47*, 11930.
(39) Liu, Y.; Chen, L.; Wu, L. M. *Inorg. Chem.* **2008**, *47*, 855.
(40) Guo, S. P.; Guo, G. C.; Wang, M. S; Zou, J. P; Xu, G.; Wang, G. J.; Long, X. F.; Huang, J. S. *Inorg. Chem.* **2009**, *48*, 7059.
(41) (a) Ok, K. M.; Chi, E. O.; Halasyamani, P. S. *Chem. Soc. Rev.* **2006**, *35*, 710. (b) Muller, E. A.; Cannon, R. J.; Sarjeant, A. N.; Ok, K. M.; Halasyamani, P. S.; Norquist, A. J. *Cryst. Growth Des.* **2005**, *5*, 1913.
(42) Setzler, S. D.; Schunemann, P. G.; Pollak, T. M.; Ohmer, M. C.; Goldstein, J. T.; Hopkins, F. K.; Stevens, K. T.; Halliburton, L. E.; Giles, N. C. *J. Appl. Phys.* **1999**, *86*, 6677.
(43) Bhar, G. C.; Smith, R. C. *Phys. Status Solidi A* **1972**, *13*, 157.
(44) (a) Jorgensen, C. K. *Orbitals in Atoms and Molecules*; Academic Press: London, 1962. (b) Amberger, H. D.; Hagen, C. *Spectrochim. Acta, Part A* **1994**, *50*, 1267. (c) Reddmann, H.; Jank, S.; Amberger, H. D. *Spectrochim. Acta, Part A* **1997**, *53*, 495. (d) Reddmann, H.; Apostolidis, C.; Walter, O.; Rebizant, J.; Amberger, H. D. *Z. Anorg. Allg. Chem.* **2005**, *631*, 1487. (e) Carnall, W. T.; Goodman, G. L.; Rajnak, K.; Rana, R. S. *J. Chem. Phys.* **1989**, *90*, 3443.
(45) (a) Savin, A.; Nesper, R.; Wengert, S.; Fässler, T. F. *Angew. Chem., Int. Ed. Engl.* **1997**, *36*, 1809. (b) Fässler, T. F. *Chem. Soc. Rev.* **2003**, *32*, 80. (c) Becke, A. D.; Edgecomb, K. E. *J. Chem. Phys.* **1990**, *92*, 5397.
(46) (a) Watson, G. W.; Parker, S. C. *J. Phys. Chem. B* **1999**, *103*, 1258. (b) Watson, G. W.; Parker, S. C.; Kresse, G. *Phys. Rev. B: Condens. Matter Mater. Phys.* **1999**, *59*, 8481. (c) Lefebvre, I.; Szymanski, M. A.; Olivier-Fourcade, J.; Jumas, J. C. *Phys. Rev. B: Condens. Matter Mater. Phys.* **1998**, *58*, 1896. (d) Huang, Y. Z.; Wu, L. M.; Wu, X. T.; Li, L. H.; Chen, L.; Zhang, Y. F. *J. Am. Chem. Soc.* **2010**, *132*, 12788.